

# Mechanism of Iron Oxide Scale Reduction in 5% H<sub>2</sub>–N<sub>2</sub> Gas at 650–900 °C

R. Y. Chen<sup>1</sup>

Received: 11 December 2016/Revised: 1 March 2017/Published online: 12 April 2017  
© Springer Science+Business Media New York 2017

**Abstract** The reduction behaviour of the oxide scale on hot-rolled, low-carbon steel strip in 5% H<sub>2</sub>–N<sub>2</sub> gas at 650–900 °C was studied. In general, the reduction rate of the oxide scale at the centre location was more rapid than that at the near-edge location. In both cases, the reduction rates at 650 °C were extremely low and the rates increased with increased temperature, reaching their maxima at 850 °C. Arrhenius plot of the rate constant derived from the early parabolic stage revealed that the reduction mechanism at 650–750 °C differed from that at 750–850 °C, with the former being oxygen diffusion in  $\alpha$ -Fe and the latter most likely iron diffusion in wustite. In all cases, a thin iron layer formed on the scale surface within a very short time and then the thickness of this layer remained essentially unchanged, while the scale layer was gradually reduced via outward migration of the inner wustite–steel interface, as a result of inward iron diffusion through the wustite layer to that interface. More rapid oxygen diffusion through the thin surface iron layer than the oxygen supply rate through interface reaction was believed to result in a lower oxygen potential at the outer iron–wustite interface, thus providing a driving force for iron to diffuse through the wustite layer. The inner wustite–iron interface became undulating initially; then with the rapid advance of some protruding sections, some parts of the wustite layer were reduced through first, and finally the remaining wustite islands were reduced to complete the reduction process. Porosities were generated when wustite islands were reduced due to localized volume shrinkage. Higher oxygen concentrations in the scales of the near-edge samples were believed to be responsible for their slower reduction rates than those of the centre location samples.

---

✉ R. Y. Chen  
rex.chen@bluescopesteel.com

<sup>1</sup> Product Innovation and Technology, BlueScope Limited, Hastings, VIC 3915, Australia

**Keywords** Oxide scale · Low-carbon steel · Wustite · Reduction · 5% $H_2$ - $N_2$  · 650–900 °C

## Introduction

Following a development Danieli made in 2000 using pure hydrogen to reduce oxide scale on hot-rolled steel strip [1, 2], there have been some renewed interests recently in studying the reduction behaviour of oxide scale on hot-rolled steel strip, in the hope of identifying a more practical operation window for further development of this technology. The early development of Danieli led to the construction of a pilot line and a commercial line with a target output rate of 120,000 metric tonnes per annum. No further development was reported thereafter. The laboratory results used in this development were reported by Primarera et al. [3] in a later paper. In this paper [3], the results showing the effect of temperature, gas dilution level and  $H_2O$  content on the reduction kinetics were reported, but some results, especially the absence of a rate minimum temperature, were inconsistent with the results reported in later studies.

During 2004–2007, under the auspices of European Commission, Picard et al. [4] conducted a three-year project, exploring options that could be used to (1) decrease oxide scale thickness during hot rolling and (2) effectively and efficiently reduce the oxide scale on hot-rolled steel strip using  $H_2$ - $N_2$  gas mixtures. The temperature range examined was 750–1100 °C. From this study, it was concluded that it was possible to reduce a 10- $\mu$ m-thick scale layer on steel using flowing 100% $H_2$  at relatively high temperatures within a short time (e.g., 2 min at 850 °C and 3 min at 750 °C). The product of the reduction reaction was a layer of sponge iron that could not be easily removed mechanically, but could be compacted by a cold-rolling step. However, the processing times required identified were considered to be too long as compared to the time required in a conventional pickling process. Also, with the high temperatures required, the post-cooling chamber would be excessively long. These made it difficult to design a compact industrial installation with a high productivity. In addition, the requirement of using 100% $H_2$  was impractical as in a continuous operation line; water vapour would be generated as a result of reaction between the scale and the hydrogen gas. No further development in the scale reduction process was planned by the European Commission after the 3-year project.

Since then, various academic studies were conducted to explore other options of oxide scale reduction. Shi et al. [5] examined the reduction behaviour of mill scale (7–8  $\mu$ m thick) on a low-carbon steel in 100% $CO$  at 710–770 °C and found that the optimal conditions were 750 °C for 3 min with a gas flow rate of 3 L  $min^{-1}$  (litres per minutes). However, it was found that carburization of the reduced iron also occurred.

Saeki et al. [6] examined the reduction behaviour of a 5- $\mu$ m-thick scale layer at 400–800 °C in 100% $H_2$ . It was found that within 400–550 °C, the reduction rate increased with increased temperature. However, there was a sudden reduction rate decrease at 600 °C, and thereafter, the reduction rate increased with increased

temperature again. Different morphologies of the reduction products were observed in this study. After reaction at 400 °C for 90 min, the reaction product was compact with the scale layer essentially unaffected. After 90 min at 500–550 °C, however, the reaction product was porous, comprising a mixture of fine-grained iron particles, porosities and probably some residual oxide particles. After 90 min at 600–700 °C, a thin white layer of metallic iron formed on the surface and the original scale layer became non-uniform in thickness. After 90 min at 800 °C, the entire scale layer was reduced to a metallic iron with some relatively large porosities in it. The observation of a rate minimum at 600 °C was interesting. It was believed that the changes in the scale morphology and the type of oxide were responsible for the sudden change in the reaction manner, but in what way these changes would have affected the reaction manner and kinetics was not discussed.

In 2014, the reduction behaviour of mill scale (7–8 μm thick) at a relatively low temperature range of 370–550 °C in 20% $H_2$ -Ar was examined by Guan et al. [7]. It was found that the reduction rate increased with temperature and a transition temperature of 410 °C was identified. Below the transition temperature, the rate increase was small, but after the transition temperature, the rate increased rapidly. The shortest duration identified for nearly completely reducing the 7-μm scale layer was 8 min at 550 °C. The authors believed that formation of metastable wustite as an intermediate product was responsible for the decrease in the activation energy below 410 °C. Porous reaction products were observed at 400–550 °C with the pore size increased with temperature. Guan et al. [8] then continued their study (reported in 2016) by comparing the reduction behaviour at 550 °C with that at 700–800 °C and examined the effect of increased hydrogen content in the atmosphere from 20 to 50%. The results of this later study revealed that increasing the reaction temperature to 700–800 °C did not increase the reduction rate. Instead, the reduction rate at 550 °C was still the greatest, although in the initial heating stage, more scale was reduced at 800 °C than at 550 °C. Increasing hydrogen content to 50% $H_2$ -Ar also increased the reduction rate with the rate increase at 550 °C being the most significant. The reaction rates at 700 °C in both atmospheres were the smallest (rate minimum). At 700–800 °C, a dense iron layer formed on the scale surface, whereas the reduced scale structure at 550 °C was porous. These results again related the formation of a dense iron layer on the surface to low reduction rates and porous scale structures to more rapid rates. Solid diffusion control was believed to be responsible for the low reduction rate at 700 °C, but what diffusion processes had controlled the reduction process was not discussed. The total duration required to completely reduce the scale was not determined in this later study.

The temperature effect was also studied by He et al. [9]. The scale structure used for this evaluation was one that corresponding to that taken from the near edge region of a hot-rolled strip [10, 11], comprising a two-layered structure with an outer magnetite layer and an inner layer of  $Fe_3O_4$ -Fe mixture. The temperature range examined was 400–900 °C, and the atmosphere used was 10% $H_2$ - $N_2$ . The results of this study were consistent with those of Saeki et al. [6] and Guan et al. [8], namely, (1) within the range of 400–500 °C, the reduction rate increased with temperature and porous reduction products were obtained, (2) there was a sudden decrease in the reduction rate at 600 °C but the rate minimum temperature was at

700 °C, (3) the reduction rate increased again with temperature within 700–900 °C. At this higher temperature range, the scale surface was covered by a thin layer of metallic iron and the reduction reaction proceeded by migration of the scale–steel interface outward, consistent with the observations made by Saeki et al. [6] and Picard et al. [4].

To accelerate the reduction process, Liu et al. [12] examined the effect of scale breaking on the reduction rate in 5% $\text{H}_2$ – $\text{N}_2$  at 600–900 °C. It was found that scale breaking significantly increased the reduction rate, but within 600–800 °C, it was still not possible to completely reduce the entire scale layer within 30 min even with a compression ratio of nearly 30%. Only when the temperature was increased to 900 °C at a compression ratio of 26%, could the scale be completely reduced within 30 min.

Some other studies [13, 14] were also conducted to assess the quality of a hot-dipped galvanized coating on partially reduced oxide scale. In preparing the surface for galvanizing, one study [13] introduced 30% compression to break the scale prior to scale reduction in 20% $\text{H}_2$ – $\text{N}_2$  at 800 °C, while the other study [14] used rapid cooling after coiling to generate a scale layer containing more than 20% wustite prior to scale reduction in an atmosphere containing more than 20% $\text{H}_2$  at 550–700 °C. It was claimed that even with the presence of scale residues on the steel surface, the galvanized coating produced could still adhere well to the steel. It is known that iron oxides are not deformable at room temperature [15]. The presence of a significant percentage of scale residues in the galvanized coating would be a significant concern to the manufacturers and their customers.

Summarizing the results of previous studies, the following conclusions can be made:

1. There is a rate minimum temperature at about 600–700 °C, below and above which, the scale reduction rate increased with increased temperature. The rate minimum temperature appears to be a function of the hydrogen content in the atmosphere.
2. The reduction product at 500–550 °C is porous, forming a spongy iron layer.
3. The reduction product above 700 °C is compact, with a thin iron layer on the surface, and the scale is reduced primarily via outward migration of the scale–steel interface.
4. The mechanisms of forming the above reduction products are not well understood, and therefore, the reason of having a rate minimum at 600–700 °C is still unknown.
5. The effect of scale structure on the reduction process has not been addressed.

The current study is therefore designed to compare the reduction behaviour of two types of oxide scale structures: one representing the structure at the centre location of the strip and the other representing the near-edge location, in different  $\text{H}_2$ – $\text{N}_2$  gas mixtures at 450–900 °C. This paper presents the results of scale reduction in 5% $\text{H}_2$ – $\text{N}_2$  at 650–900 °C.

## Experimental Procedures

Oxide scales formed on a hot-rolled steel strip containing 0.055C–0.23Mn–0.012Si with a thickness of 7–8  $\mu\text{m}$  are used in the current study. Figure 1 shows the locations where the scale samples were taken. It was determined in a previous study [10] that the scale structures at these locations were different, with the structure at the centre region comprising a mixture of  $\text{Fe}_3\text{O}_4$ –Fe and that at the near-edge location having a two-layered structure with an outer layer of  $\text{Fe}_3\text{O}_4$  and an inner layer of  $\text{Fe}_3\text{O}_4$ –Fe mixture. The steel samples were sectioned to  $25 \times 20$  mm coupons for the reduction experiments.

The experiments were conducted in a horizontal tube furnace. High-purity nitrogen and premixed 5% $\text{H}_2$ – $\text{N}_2$  gases supplied by BOC Australia were used. In a typical experiment, the sample was loaded to the reaction zone after the target temperature was reached. Preheating to the target temperature usually required 8–10 min. During preheating, high-purity nitrogen was used to prevent oxidation. It was observed that there was a slight weight loss during preheating. A dummy sample was then used for each temperature to record this weight loss, which was used to calculate the true weight loss of the reduction reaction. A thermocouple with its tip located near the sample was used to monitor the sample temperature. Upon reaching the target temperature, 5% $\text{H}_2$ – $\text{N}_2$  flowing at  $3 \text{ L min}^{-1}$  was turned on to replace the high-purity nitrogen flow. For the temperature range of 650–900  $^\circ\text{C}$ , the gas flow rate in the range of 0.8–3  $\text{L min}^{-1}$  was found to have little effect on the reaction rate. Therefore, the experiments were conducted in a flow rate of  $0.8 \text{ L min}^{-1}$  (corresponding to a linear velocity of  $0.8 \text{ cm s}^{-1}$  at room temperature) after the first minute flowing at  $3 \text{ L min}^{-1}$ . At the end of each experiment, high-purity nitrogen flowing at a rate of  $5 \text{ L min}^{-1}$  was turned on to replace the reaction gas flow, and the sample was withdrawn to the cold zone for cooling. After the sample was cooled to a temperature below 150  $^\circ\text{C}$ , it was removed from the furnace. The weight loss calculated by the weights measured before and after the experiment was used to calculate the amount of scale reduced. Repeated experiments were conducted for some conditions to confirm the results.

After the experiments, optical and scanning electron microscopies (SEM) equipped with EDS (energy dispersive spectroscopy) were used to examine/characterize selective samples. SEM images are not presented because it was found that optical images could reveal sufficient details and provided better colour

**Fig. 1** Locations of steel samples taken for reduction experiments. *Region A*: strip centre—the scale comprises a mixture of  $\text{Fe}_3\text{O}_4$ –Fe throughout its thickness, and *Region B*: near-edge location—the scale has two layers, with an outer layer of  $\text{Fe}_3\text{O}_4$  and an inner layer of  $\text{Fe}_3\text{O}_4$ –Fe mixture [10]

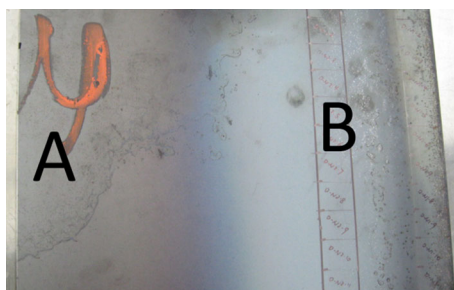


**Fig. 2** Selected images of scale samples after reduction experiments: **a** centre, 650 °C, **b** centre 700 °C, **c** near edge, 700 °C, **d** centre, 750 °C, **e** near edge, 750 °C, **f** near edge, 800 °C, **g** near edge, 850 °C and **h** centre, 900 °C

contrasts between the iron layer (bright) and the wustite phase (dark grey). More experimental details are reported elsewhere [16].

## Results

Upon exposure to the reduction gas at all temperatures, the scale surface was quickly covered with a layer of metallic iron and this colour appearance did not change for longer exposure times, as shown in Fig. 2. The shortest times required to obtain complete coverage of metallic iron on the surface for all temperatures are listed in Table 1. It is seen that while the times were all very short, the time required for the metallic iron to cover the near-edge samples was longer, but in all cases, the durations were no more than 2 min.

The reduction rates for the scales at both locations are compared in Figs. 3 and 4. Figures 3a and 4a compare the reduction kinetics within 60–90 min, whereas Figs. 3b and 4b show the results for 4 h and longer. Note that the maximum amounts of scale in each group of samples may differ, because they were taken from different locations. When the weight loss curve starts to plateau, it indicates that the scale is nearly completely reduced. We define the time when the weight loss curve starts to plateau as the reduction completion time. The reduction completion times for all samples are summarized in Table 2.

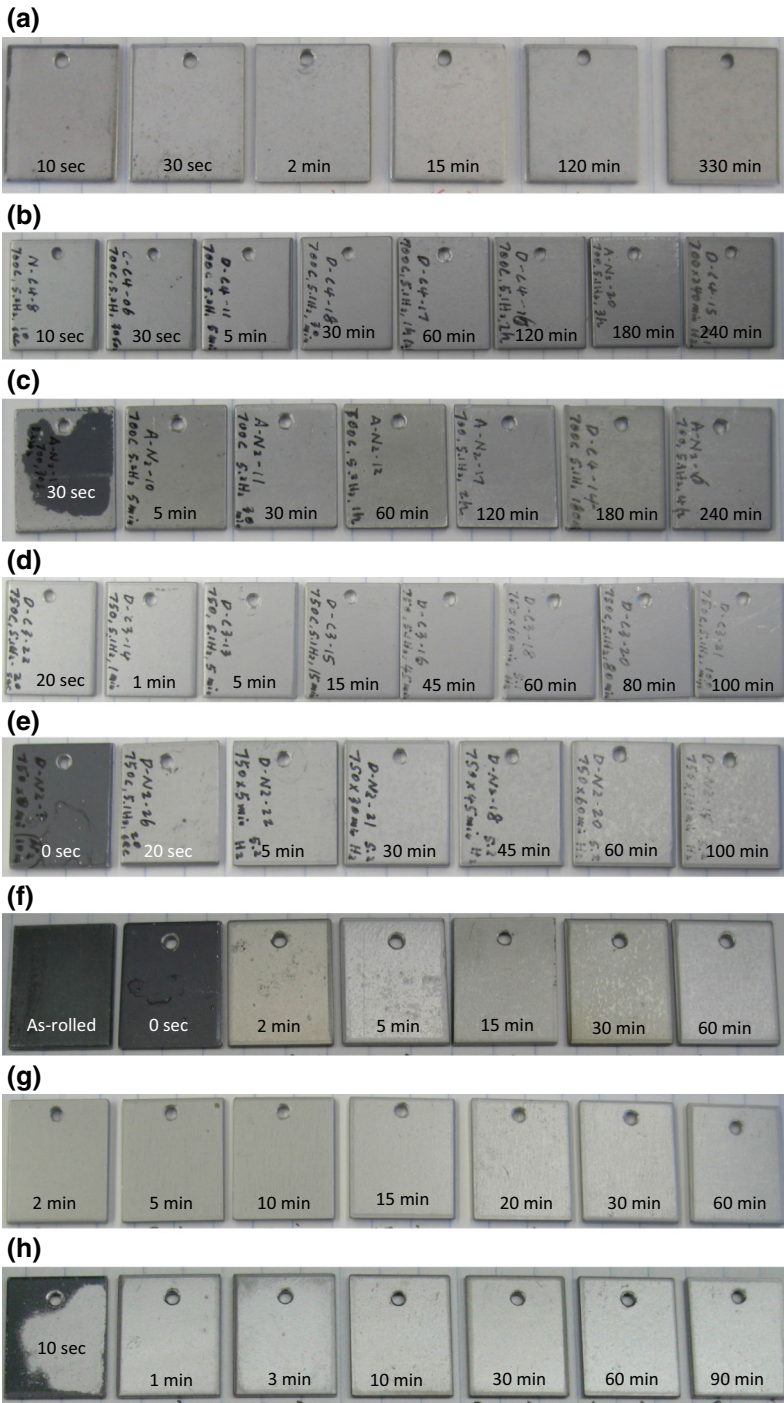
Figures (3, 4) and Table 2 show that, in general, (1) the scale at the centre location was easier to reduce than that at the near-edge location. For example, the completion time at 850 °C for the centre sample was 20 min, less than half of the time required for the near-edge sample (45 min); (2) the reduction rates increased with temperature to their maxima at 850 °C; (3) the reduction rates at 650–700 °C were extremely slow: at 700 °C, the completion time was 4 h or longer, and an even longer time (>10 h) was required at 650 °C, and (4) the reduction rates at 900 °C were initially about the same as those at 850 °C but the rates decreased at a later stage.

Parabolic plot of the kinetics data (Figs. 5, 6) revealed that the early stage kinetics for both groups of samples was closely parabolic, suggesting that solid-phase diffusion could be the control mechanism. Regression of the kinetics data using the following equation,

$$W^2 = k_p t + C \quad (1)$$

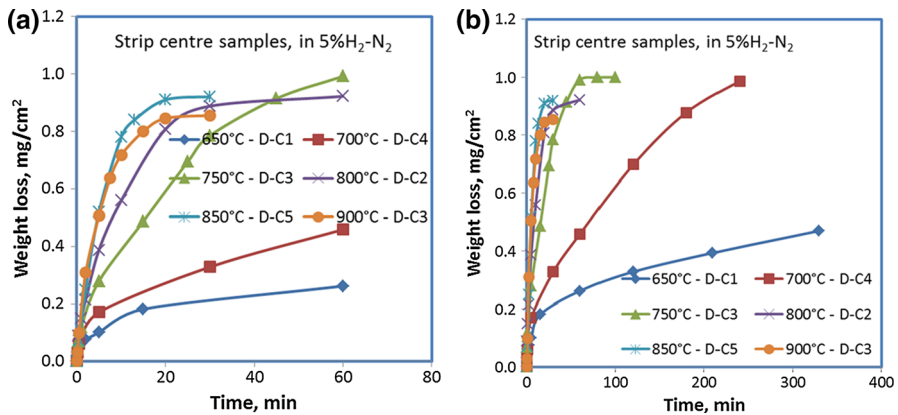
where  $W$  is the weight gain per unit surface area in  $\text{mg cm}^{-2}$ ,  $t$  is reduction time in min, and  $C$  is a constant, yields the rate constant  $k_p$  data (in  $\text{mg}^2 \text{cm}^{-4} \text{min}^{-1}$ ), as listed in Table 3.

Arrhenius plots of the data in Table 3 are shown in Fig. 7. It is seen that the mechanism controlling the kinetics at 650–750 °C appeared to be different from that



**Table 1** Time required for complete coverage of the surface with an iron layer

Temperature (°C)	Time ( <i>t</i> )	
	Centre	Near edge
650	$t < 10$ s	$30 \text{ s} < t < 1$ min
700	$t < 10$ s	$30 \text{ s} < t < 2$ min
750	$10 \text{ s} < t < 20$ s	$30 \text{ s} < t < 2$ min
800	$t < 20$ s	$30 \text{ s} < t < 2$ min
850	$t < 20$ s	$20 \text{ s} < t < 1$ min
900	$40 \text{ s} < t < 1$ min	$40 \text{ s} < t < 1$ min

**Fig. 3** Reduction kinetics of the scale taken at the strip centre location: **a** within the first 60 min and **b** for longer experimental durations

at the higher temperature range. Linear regression of the kinetics data shown in Fig. 7 yields the following rate constant expressions and the activation energies obtained are listed in Table 4.

For the centre samples at 650–750 °C:

$$k_P = 3.01 \times 10^{11} \exp \left[ \frac{-259840 \left( \frac{\text{J}}{\text{mol}} \right)}{RT} \right] \text{ mg}^2 \text{ cm}^{-4} \text{ min}^{-1} \quad (2)$$

For the centre samples at 750–850 °C:

$$k_P = 1.87 \times 10^5 \exp \left[ \frac{-138500 \left( \frac{\text{J}}{\text{mol}} \right)}{RT} \right] \text{ mg}^2 \text{ cm}^{-4} \text{ min}^{-1} \quad (3)$$

For the near-edge samples at 650–750 °C:

$$k_P = 5.63 \times 10^{11} \exp \left[ \frac{-264520 \left( \frac{\text{J}}{\text{mol}} \right)}{RT} \right] \text{ mg}^2 \text{ cm}^{-4} \text{ min}^{-1} \quad (4)$$

For the near-edge samples at 750–850 °C:



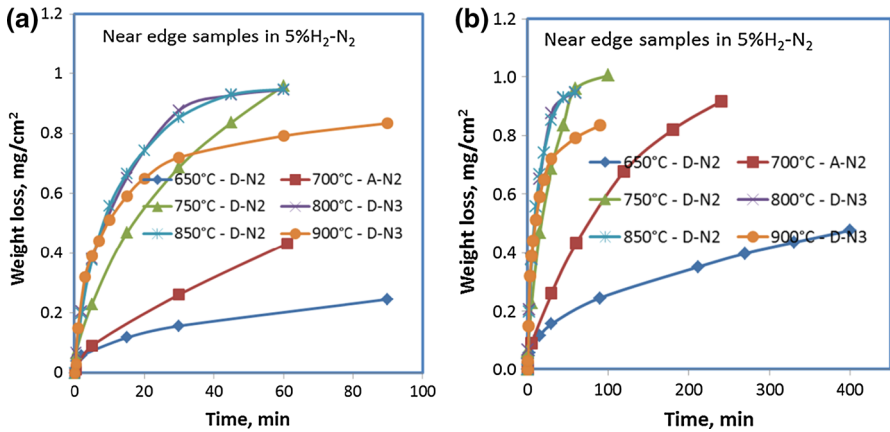


**Fig. 4** Reduction kinetics of the scale taken at the near-edge location: **a** within the first 90 min and **b** for longer experimental durations

**Table 2** Reduction completion time

Temperature (°C)	Centre (min)	Near edge (min)
650	≫330	≫390
700	240	>240
750	60	90
800	30	45
850	20	45
900	20	>90

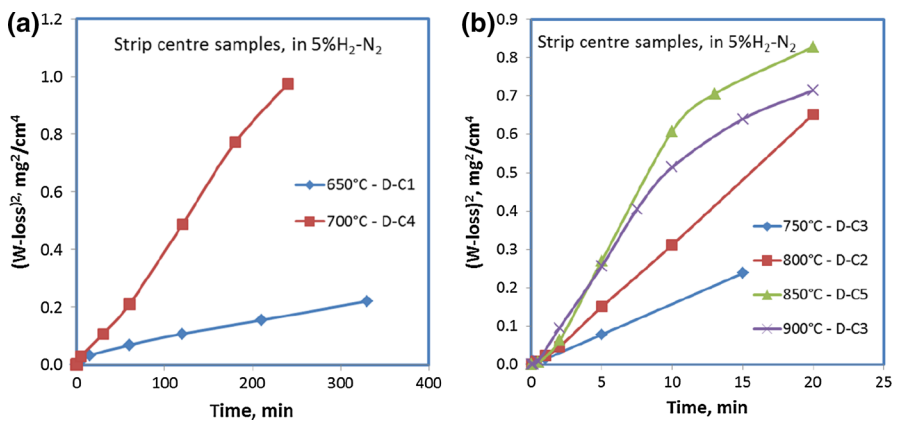


**Fig. 5** Parabolic plot of the early stage kinetics data shown in Fig. 3 for strip centre samples: **a** 650–700 °C and **b** 750–900 °C

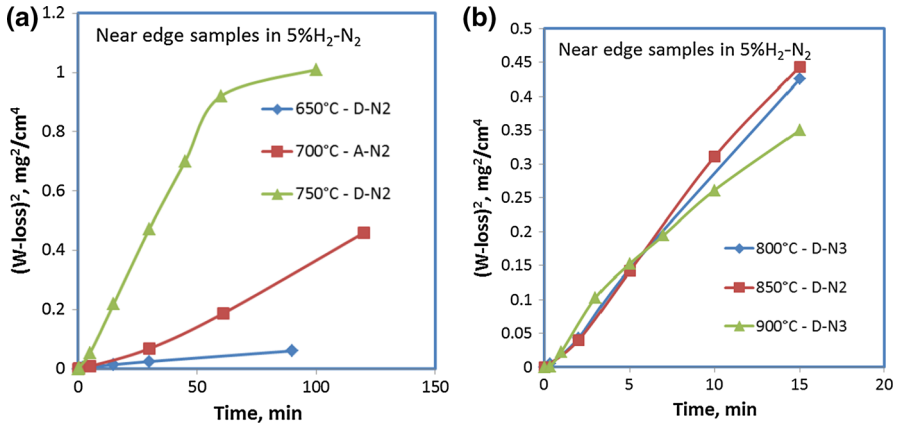


**Fig. 6** Parabolic plot of the early stage kinetics data shown in Fig. 4 for near-edge samples: **a** 650–750 °C and **b** 800–900 °C

**Table 3** Parabolic rate constants obtained from the early stage of reduction

Temperature (°C)	$k_p$ ( $mg^2\ cm^{-4}\ min^{-1}$ )	
	Centre	Near edge
650	$5.86 \times 10^{-4}$	$5.50 \times 10^{-4}$
700	$3.52 \times 10^{-3}$	$4.38 \times 10^{-3}$
750	$1.60 \times 10^{-2}$	$1.58 \times 10^{-2}$
800	$3.36 \times 10^{-2}$	$2.89 \times 10^{-2}$
850	$6.82 \times 10^{-2}$	$3.39 \times 10^{-2}$
900	$5.59 \times 10^{-2}$	$2.25 \times 10^{-2}$

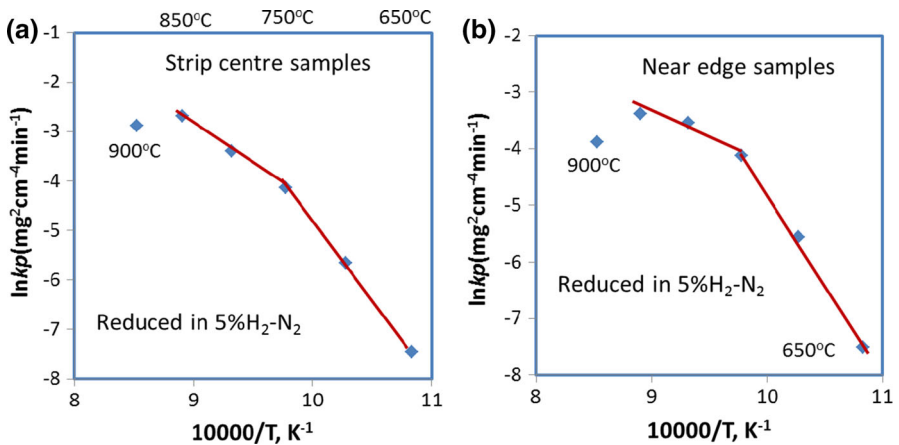


**Fig. 7** Arrhenius plots of the rate constants in Table 3: **a** for strip centre samples and **b** for near-edge samples

**Table 4** Comparison of activation energies

Sample	Temperature	Activation energy (kJ mole <sup>-1</sup> )	References
Centre	650–750 °C	259.8	This work
	750–850 °C	138.5	This work
Near-edge	650–750 °C	264.5	This work
	750–850 °C	73.55	This work
Iron diffusion in Fe <sub>0.907</sub> O	700–900 °C	124.3	[43]
Iron diffusion in Fe <sub>0.94</sub> O–Fe <sub>0.88</sub> O	900–1100 °C	122.9–143.3	[44, 45]
Oxygen in $\alpha$ -Fe	700–910 °C	238.5	[41, 42]
Hydrogen in $\alpha$ -Fe	20–770	3.84	[27]
Hydrogen in $\alpha$ -Fe	20–770	4.0	[28]

$$k_p = 95.8 \times \exp \left[ \frac{-73,550 \left( \frac{\text{J}}{\text{mol}} \right)}{RT} \right] \text{ mg}^2 \text{ cm}^{-4} \text{ min}^{-1} \quad (5)$$

The activation energies within the range of 650–750 °C for both the centre and edge samples are similar at about  $E_A = -260,000 \text{ J mole}^{-1}$ , whereas the  $E_A$  values at 750–850 °C are significantly smaller, suggesting that different mechanisms could be operating at different temperature ranges. In addition, the mechanisms controlling the reactions at 900 °C for both samples could be also different from those at 650–850 °C.

Selective scale structures obtained are compared in Figs. 8, 9, 10, 11 and 12. The sequence of scale structure development is systematically shown in Figs. 10 and 11 for the reduction of the centre and near-edge samples, respectively, at 800 °C. Different microscopic features are marked in selective images in Figs. 10 and 12. Upon exposure to the reduction atmosphere, an extremely thin metallic iron layer formed on the scale surface. This metallic layer was too thin to see in some optical micrographs and remained very thin throughout the reduction process. Instead of via thickening of the surface iron layer, the scale reduction process proceeded in the form of non-uniform scale–steel interface migration outward. Initially, the wustite–steel interface (then wustite–iron interface) became wavy or undulating (Fig. 10a). This was followed by outburst of metallic iron into the scale layer (Fig. 10b, c) and with longer time exposure, metallic iron started to occupy the entire scale layer at certain locations and divided the scale layer into scale islands surrounded by reduced iron (Fig. 10d), and finally, the entire scale layer was reduced to iron by consumption of the wustite islands (Fig. 10e). With the consumption of the wustite islands, cavities were left inside the reduced iron layer and the original scale layer became a mixture of reduced iron and cavities.

For the reduction in the near-edge scale at 900 °C, the iron layer on the surface appeared to thicken more than those developed under other conditions and the number of cavities left in the metallic iron layer was significantly fewer and the volume fraction of cavities was smaller (Fig. 12e–f).

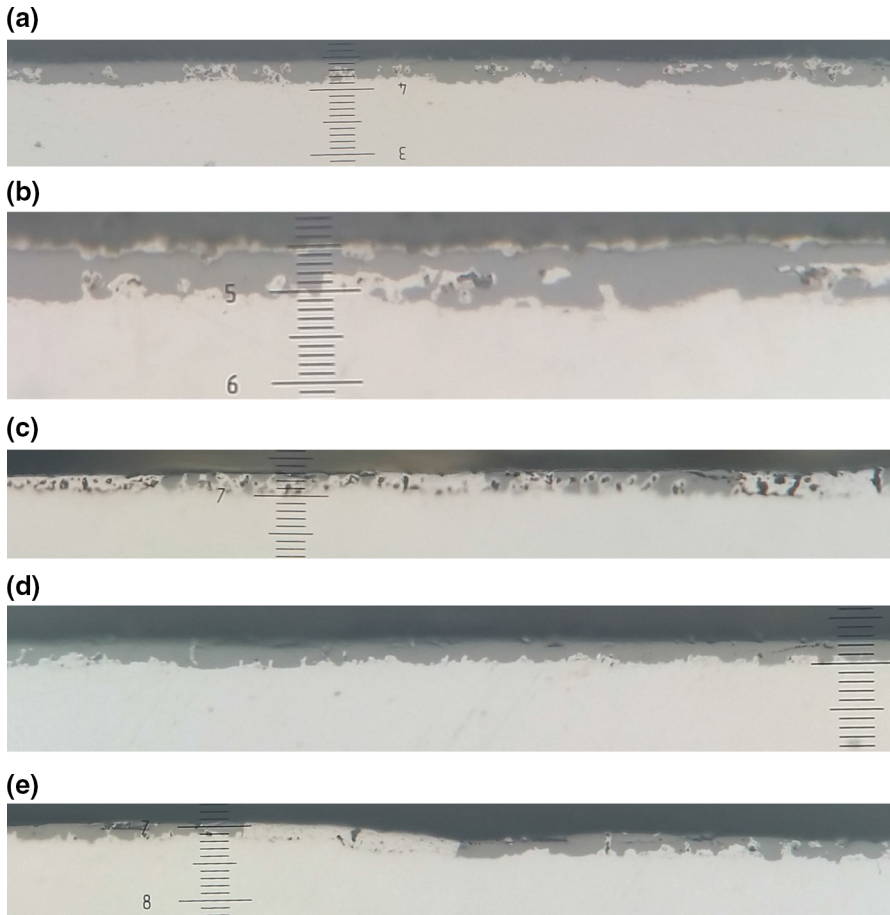


**Fig. 8** Selected scale structures after reduction at 650–700 °C: **a** centre sample, 650°C × 120 min, ×500, **b** centre sample, 650°C × 330 min, ×1000, **c** centre sample, 700°C × 240 min, ×500, **d** near-edge sample, 700°C × 30 min, ×500 and **e** near-edge sample, 700°C × 120 min, 500X

Figure 13 gives a schematic illustration of the reduced scale structure development throughout the reduction process. Such a reduction pattern was seen at all temperatures (650–900 °C) and on both types of scales (Figs. 8, 9, 10, 11, 12).

## Discussion

The observation of a persistently thin metallic iron layer on the scale surface, followed by outward migration of the wustite–steel interface to complete the reduction process, was surprising. One would have expected that the reduction process would have started from the scale surface, forming a layer of reduced iron, and then, the reduced iron layer would have thickened by consuming the scale layer gradually from the surface inwards and eventually replacing the entire scale layer

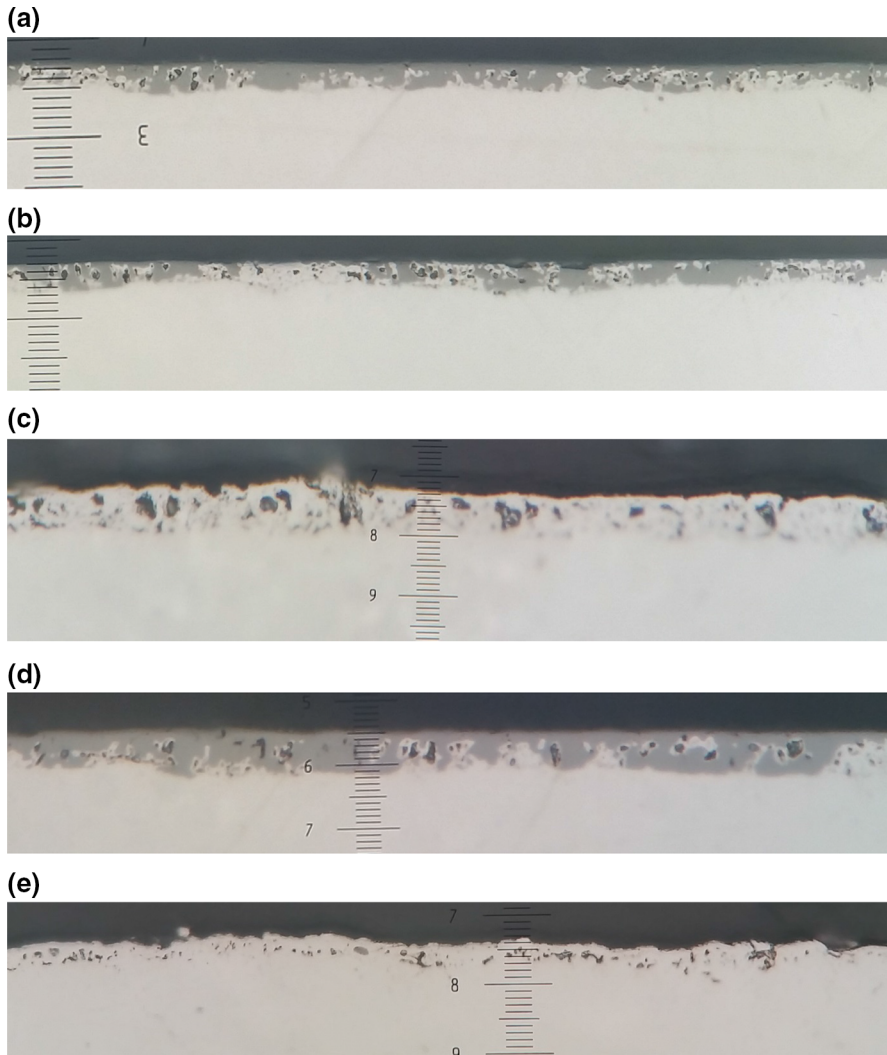


**Fig. 9** Selected scale structures after reduction at 750 °C: **a** centre sample, 5 min,  $\times 500$ , **b** centre, 15 min,  $\times 500$ , **c** centre sample, 100 min,  $\times 1000$ , **d** near-edge sample, 5 min,  $\times 1000$  and **e** near-edge sample, 60 min,  $\times 500$

with reduced iron. However, the actual observations made have contradicted this expectation.

In the search for an answer, it was found that this apparently peculiar phenomenon was observed nearly 70 years ago by Gellner and Richardson [17], who studied the reduction behaviour of a wustite layer formed on pure iron in pure hydrogen at 600–1060 °C. In that study, it was found that at 700 °C, reduction in the wustite layer proceeded from the surface inwards as expected, forming a spongy iron layer as the reduction product, whereas at 900 °C, a very thin film of iron

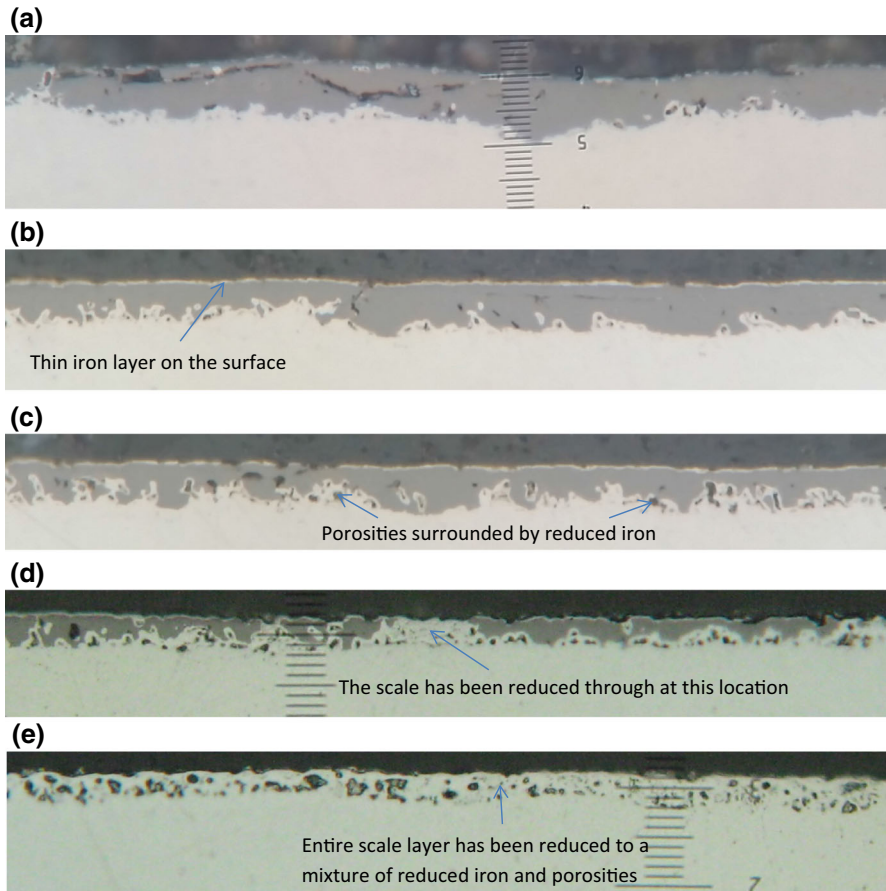


**Fig. 10** Selected centre location scale structures after reduction at 800 °C for: **a** 1 min,  $\times 1000$ , **b**, **c** 5 min, at two different locations,  $\times 1000$ , **d** 30 min,  $\times 500$  and **e** 60 min,  $\times 500$

formed on the wustite surface first, then its growth soon ceased and the subsequent reduction process proceeded outward from the inner iron–wustite interface. Interestingly though, Turkdogan and Vinters could not observe the same phenomenon in their later study of the reduction in partially oxidized iron strips in pure hydrogen at 700–1200 °C [18]. The reason for this is unknown.

The observations made in the current study are consistent with that observed by Gellner and Richardson [17] at 900 °C, but the temperature range where this phenomenon is present has extended to 650 °C.

In interpreting their observation at 900 °C, Gellner and Richardson [17] believed that there could be an oxide stability gradient across the wustite layer with the inner wustite–iron interface being the least stable and the outer iron–wustite being the most stable. Based on this assumption, the authors proposed that the reduction process followed the following course: (1) removal of oxygen by hydrogen from the surface of the oxide with resultant supersaturation of the oxide with iron; (2)

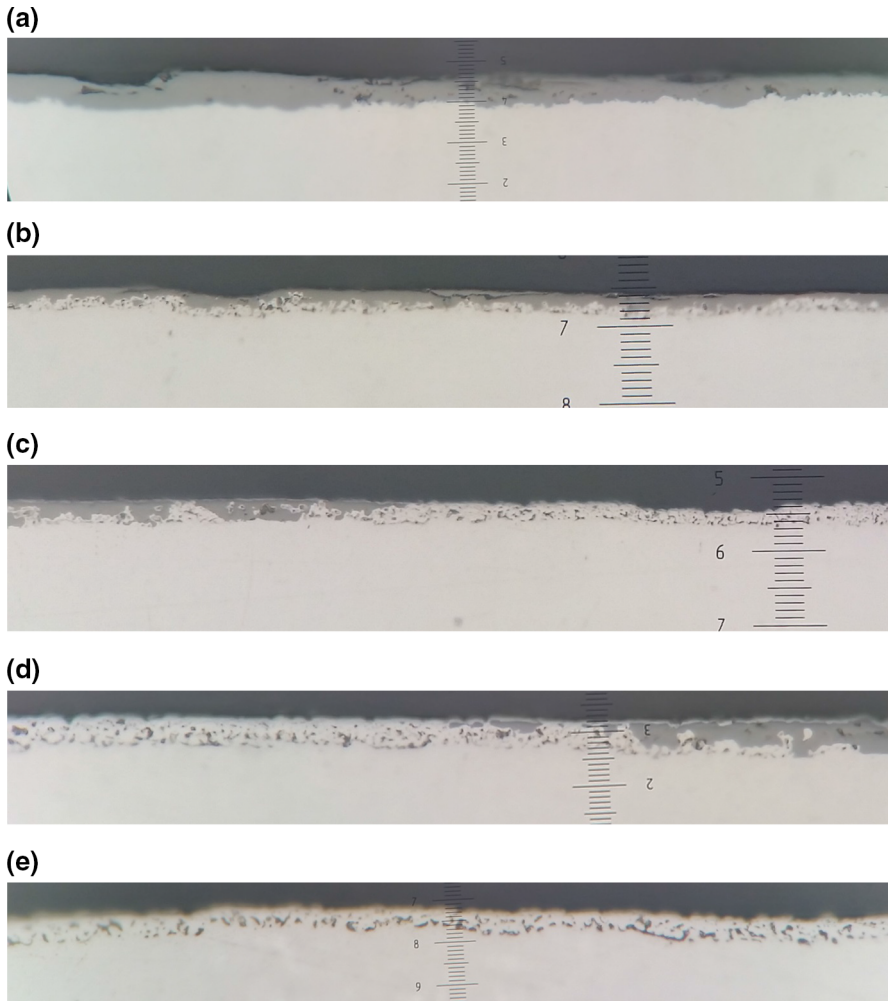


**Fig. 11** Selected near-edge scale structures after reduction at 800 °C for **a** 0 min, **b** 2 min, **c** 15 min, **d** 30 min and **e** 60 min. All at  $\times 500$

nucleation of this excess iron to form a thin layer of metal on the surface; (3) retardation of further reduction by the surface metal, which restricts access of hydrogen to the oxide and the diffusion of water vapour away from it; (4) diffusion of the excess iron, produced in the outermost layers of oxide by the continuing reduction, into the body of the oxide; (5) when the temperature is high enough and the diffusion rapid enough, preferential growth of massive iron outward from the base metal, where the oxide is the least stable. While these five steps explained well the observation, the assumption that the oxide at the inner scale-iron interface was the least stable appeared to be questionable because with the presence of a reducing atmosphere on the surface, it would be difficult to believe that the wustite-iron

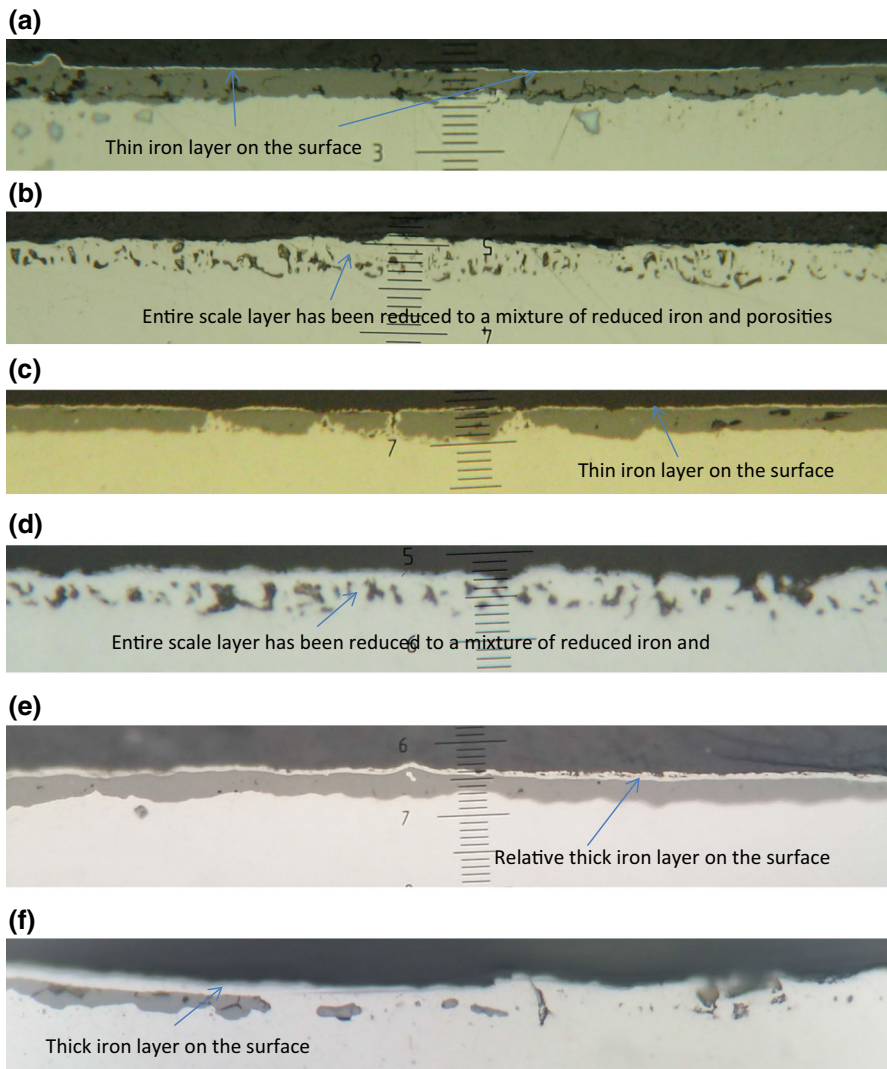


**Fig. 12** Selected scale structures after reduction at 850–900 °C: **a** centre sample, 850 °C × 2 min, **b** centre sample, 850 °C × 30 min, **c** centre sample, 900 °C × 2 min, **d** centre sample, 900 °C × 10 min, **e** near-edge sample, 900 °C × 10 min and **f** near-edge sample, 900 °C × 30 min. All at ×500

interface further away from the atmosphere would have been more unstable than that nearer to the atmosphere.

A slightly different observation was made by Richardson and Dancy [19] in another study, where it was found that during reduction in an oxide layer of about 100,000 lattice spacings, metallic iron was not formed on the surface as the reduction proceeded, but that the surface continued to consist of iron oxide for over half of the total period of reduction. The results suggested that following the



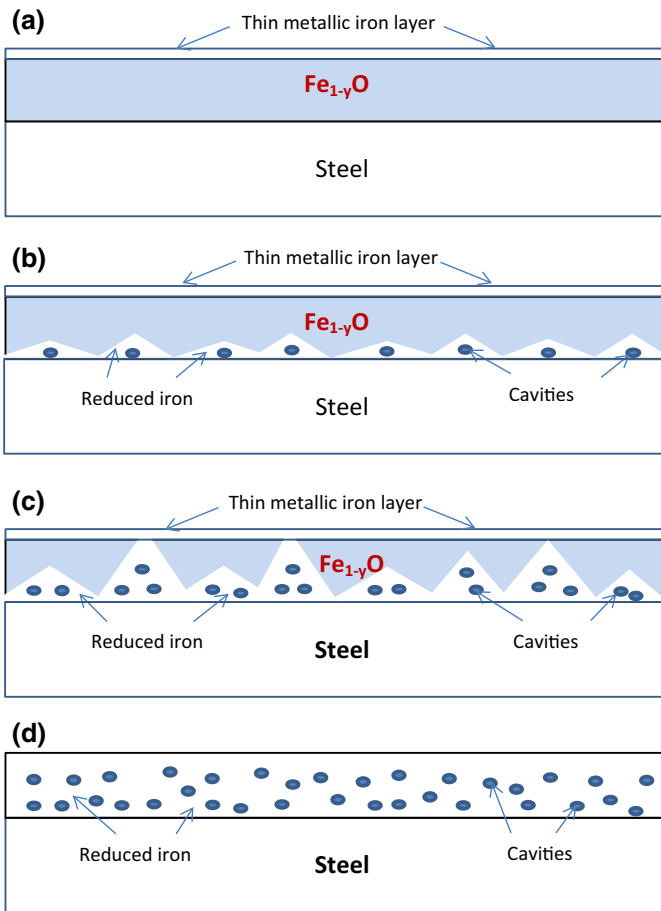
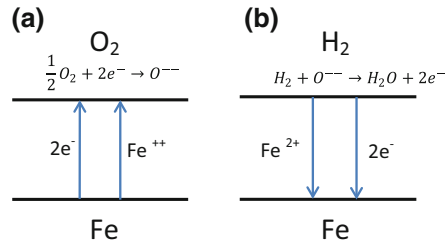


**Fig. 13** Schematic illustration of the reduction process: **a** formation of a thin iron layer on the surface, **b** development of a wavy wustite–reduced iron interface, **c** some areas of the scale were reduced through first and **d** entire scale layer was reduced to a mixture of reduced iron and cavities

removal of oxygen from the surface by the hydrogen gas, the excess iron atoms preferred to migrate through the wustite lattice and deposited on the central metallic iron before they could nucleate to form a separate phase on the surface. They believed that such a phenomenon was associated with the high vacancy concentration (5%) in wustite. It would be possible that during reduction, a concentration gradient of vacant lattice sites was built up across the wustite layer with the value being low at the surface, and 5% at the scale-iron core interface. A steady movement of iron ions could then take up this gradient towards the iron core and such a process appeared to be rapid enough to prevent the excess iron nucleation to form a separate phase on the surface initially. For this observation, an explanation was given by Hoar using a model analogical to steel oxidation as shown in Fig. 14 [20]. In this model, Hoar believed that the wustite reduction process was opposite to

**Fig. 14** Hoar's models showing mechanisms of **a** steel oxidation by oxygen forming wustite and **b** wustite reduction to iron by hydrogen [20]



the iron oxidation process, with the former having hydrogen as the reaction gas and the latter having oxygen as the reaction gas.

Wagner [21] also provided a description and interpretation of the observation made by Geller and Richardson at 900 °C [17] with an emphasis on how the metallic iron nucleates and grows into a continuous layer. He believed that there was a quasi-steady state with the following consecutive reactions: (1) phase-boundary reaction at the surface of the oxide with the reducing agent by which either excess cations and electrons are formed, or cation vacancies and electron holes are filled up. (2) Diffusion of cations and electrons towards the base of the metallic nuclei in contact with oxide. (3) Phase-boundary reaction at the interface between oxide and metal, i.e., transfer of cations and electrons into the metallic phase. Surprisingly, while acknowledging and describing in details how the surface metallic iron layer would nucleate and grow, Wagner did not discuss the subsequent processes following the formation of a metallic iron layer. Clearly, the interpretation given by Wagner is more suitable for explaining the observations made by Richardson and Dancy [19] where a continuous layer of metallic iron has not formed on the surface. Edström also had a brief discussion of the reduction mechanism with general agreement with those of Wagner [22].

The observations made in the current study are consistent with that of Geller and Richardson at 900 °C [17] as we observed that a metallic iron layer swept through the surface within a very short time (within 20 s to 2 min), although the duration required was longer for the near-edge samples. From the observations made and after taking into consideration of the views of others, the reduction process observed in the current study appears to follow several consecutive steps, as discussed below.

(1) Transformation of the scale into a single wustite layer.

It is known [10, 11] that the scale structure at the centre location typically comprises a single layer of  $\text{Fe}_3\text{O}_4$ -Fe mixture, whereas the scale at the location near the edges comprises an outer layer of magnetite and an inner layer of  $\text{Fe}_3\text{O}_4$ -Fe mixture. The scale structure difference determines their different oxygen concentrations, as shown in the Fe-O phase diagram in Fig. 15 [23]. For the scale taken at the strip centre location, the oxygen content should be one that corresponding to that near the left-hand side boundary (= <51.38 at%) because during slow cooling in the steel coil after rolling, due to depletion of oxygen at the centre locations, the iron content in the wustite layer would have been equalized with the steel substrate

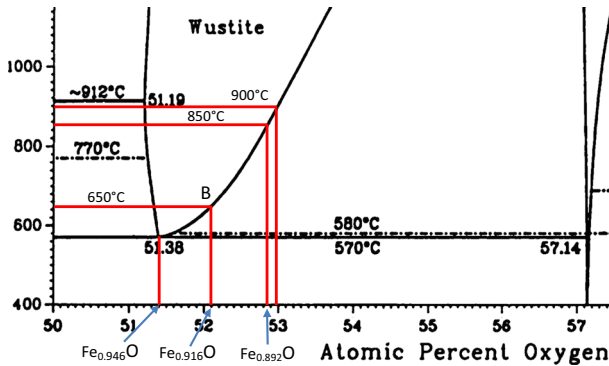


Fig. 15 Partial Fe–O phase diagram [23]

[10, 11]. Upon heating to a temperature above 600 °C, such a structure would be transformed into a single wustite layer quickly with a nearly constant oxygen concentration across its thickness [24].

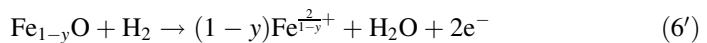
As with the scale near the strip edges, oxygen ingress to the strip edge regions during cooling after coiling had allowed the formation of a thin magnetite layer on top of the wustite layer, and consequently, the average oxygen content of the scale is located at a point between the eutectoid point of 51.38 at% and the magnetite composition of 57.14 at%, depending on the relative thickness of the magnetite layer. Upon heating to the reduction temperature, the magnetite layer would react with the adjacent wustite phase to form an oxygen-rich wustite. Depending on the reduction temperature, the composition of this oxygen-rich wustite could vary from 52.1 at% at 650 °C to nearly 53 at% at 900 °C (Fig. 15). If the magnetite layer was thin, it would be converted into oxygen-rich wustite completely. As a result of this, an oxygen concentration gradient would develop in the wustite layer with its lowest concentration at the wustite–steel interface and highest on the surface, as will be later shown in Fig. 23a.

(2) Initial reaction to form a continuous iron layer on the surface.

Upon exposure of the oxide scale to 5%H<sub>2</sub>–N<sub>2</sub> gas, hydrogen reacted with the oxygen component of the oxide to form water vapour:



The alternative expression of Eq. (6) is,



In the case of centre sample reduction, because its oxygen content is relatively low and close to the equilibrium level of 51.38 at%, Reaction (6) would result in supersaturation of iron at the surface layer of wustite quickly. When the excess iron could not diffuse away quickly, it would nucleate to form metallic iron which would then grow via iron surface diffusion as discussed by Wagner [21]. As a result, the

surface would be covered by a layer of metallic iron quickly. In the current study, the iron layer nucleated near the edge facing the hydrogen flow (Fig. 2c, h) and then swept over the entire surface, as illustrated in Fig. 16a, within 10–20 s at 650–850 °C and 40–60 s at 900 °C.

In the case of near-edge sample reduction, its surface either had an oxygen concentration >51.38 at% or was covered with a thin magnetite layer initially (Fig. 16b). In the former, upon exposure of the oxide scale to hydrogen, Reaction (6) would first remove the excess oxygen from the surface before it became supersaturated with iron. In the latter, the thin magnetite layer would be reduced to wustite first; then, the excess oxygen would be removed as the second step and finally the wustite would become supersaturated with iron to allow metallic iron to nucleate and grow in a manner similar to that of centre location samples (Fig. 16b). As a result of the additional steps involved, the duration for metallic iron to cover the entire scale surface would be expected to be longer, as also observed in the actual experiments (Table 1).

- (3) Continuation of the reduction process by outward diffusion of oxygen through the thin iron layer to the surface to react with hydrogen, assisted by iron diffusion through the wustite layer.

After the formation of the surface iron layer, direct contact between the reduction gas and the oxide was terminated. However, the reduction process continued and essentially followed the parabolic rate law at the early stage, as shown in Figs. 3, 4, 5 and 6.

The most peculiar phenomenon revealed was that the surface iron layer remained very thin throughout the reduction process at all reaction temperatures, while the oxide layer was consumed gradually by outward migration of the inner wustite–steel (then wustite–iron) interface. The immediate interpretation of this observation, following the arguments of previous researchers [17, 19–21], was that excess iron

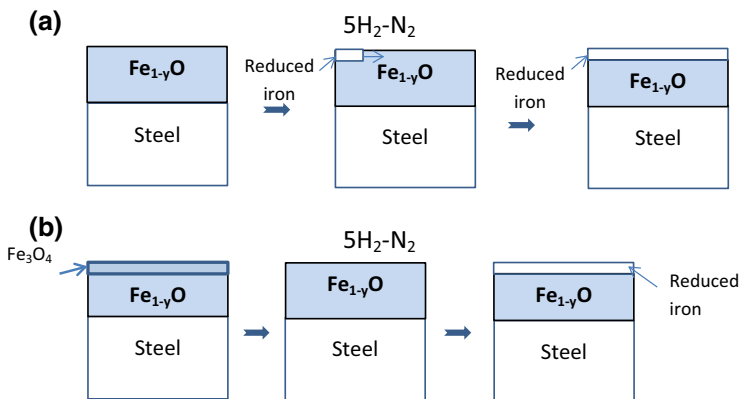


**Fig. 16** Schematic illustration of the initial reduction period for **a** centre location samples and **b** near-edge samples

ions, generated at the outer iron–wustite interface, diffused through the wustite layer and deposited in the inner iron core.

However, from the thermodynamic point of view, after the formation of an iron layer on the surface, if both of the outer and inner iron–wustite interfaces had reached the same degree of local equilibrium, then the oxygen potentials at these two interfaces would have been identical and there would have no driving force for iron to diffuse from one interface towards another.

To determine the controlling mechanism for the reduction process, Hoar’s model (Fig. 14) [20] was modified to include a layer of iron on the wustite surface in Fig. 17 to illustrate the possible reaction steps involved. As compared with Fig. 14, two additional diffusion processes, inward diffusion of hydrogen atoms [H] and outward diffusion of oxygen atoms [O] through the surface iron layer, have been added.

Although the solubility of hydrogen in iron is extremely low at room temperature, it increases rapidly with temperature [25, 26]. In addition, the diffusivity of hydrogen in  $\alpha$ -iron is relatively high at about  $10^{-4} \text{ cm}^2 \text{ s}^{-1}$  at 650–900 °C [25, 27–29]. This equates to a diffusion distance of  $x = \sqrt{Dt} = 0.01 \text{ cm}$ , or 100  $\mu\text{m}$ , per second. In other words, with its rapid diffusion rate, hydrogen can dissolve and saturate in the thin iron layer (less than 1  $\mu\text{m}$  thick) quickly.

However, if water vapour, the reaction product between hydrogen and the wustite, cannot form and escape, Reaction (6) cannot proceed. The presence of saturated hydrogen in the surface iron layer does not result in a lower oxygen activity or equilibrium oxygen potential at the iron–wustite interface. Therefore, even at the saturated level, dissolve hydrogen had no effects on the reduction process.

Reduction of bulk wustite and other iron oxides had attracted many previous studies [30–34]. It was found that when pure wustite was exposed to a reducing atmosphere ( $\text{H}_2\text{--H}_2\text{O}$  or  $\text{CO--CO}_2$  mixture), no matter what reaction product was finally obtained, a dense iron layer always formed on the wustite surface first. The formation of this dense iron layer had a profound negative effect on the reduction

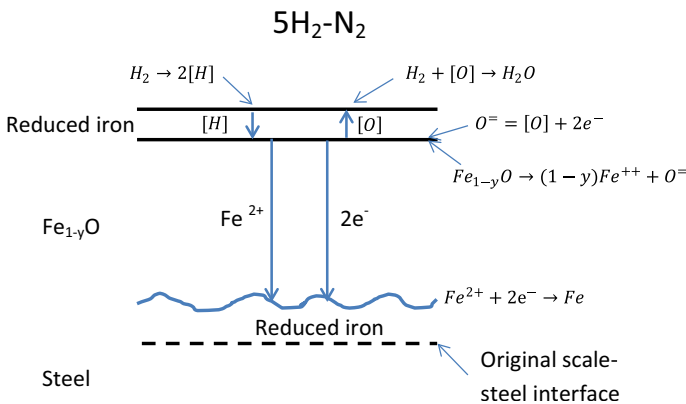


**Fig. 17** Possible diffusion processes and reactions involved in the reduction of wustite scale to iron

kinetics, because in the subsequent process, the remaining oxygen in the bulk oxide could be removed only by slow oxygen diffusion through the iron layer.

From the Fick's first law, the diffusion flux of oxygen from the iron–wustite interface to the iron surface,  $J_{\text{O}}^{\text{Fe}}$ , is expressed as,

$$J_{\text{O}}^{\text{Fe}} = D_{\text{O}}^{\text{Fe}} \frac{C_{\text{O}}^{\text{Fe-FeO}} - C_{\text{O}}^{\text{Fe-Gas}}}{x} \text{ moles cm}^{-2} \text{ s}^{-1} \quad (7)$$

where  $C_{\text{O}}^{\text{Fe-FeO}}$  = the oxygen concentration in iron in equilibrium with thermodynamically stable wustite ( $\text{moles cm}^{-3}$ ),  $C_{\text{O}}^{\text{Fe-gas}}$  = the oxygen concentration in iron at the gas–iron interface ( $\text{moles cm}^{-3}$ ),  $D_{\text{O}}^{\text{Fe}}$  = the diffusion coefficient of oxygen in solid iron ( $\text{cm}^2 \text{ s}^{-1}$ ), and  $x$  = the thickness of the dense iron layer, cm.

In the presence of hydrogen at the gas–iron interface,  $C_{\text{O}}^{\text{Fe-FeO}} \gg C_{\text{O}}^{\text{Fe-Gas}}$ , and Eq. (7) is reduced to:

$$J_{\text{O}}^{\text{Fe}} = D_{\text{O}}^{\text{Fe}} \frac{C_{\text{O}}^{\text{Fe-FeO}}}{x} \text{ moles cm}^{-2} \text{ s}^{-1} \quad (7')$$

Since the solubility [35–37] and diffusivities [35–39] of oxygen in solid iron are very low, the reduction rate of bulk wustite following the formation of a surface iron layer was significantly lowered, and from Eq. (7'), the oxygen flux is inversely proportional to the iron layer thickness. As a result of this, the subsequent reduction process becomes extremely slow and difficult [34].

As compared to the situation of bulk wustite reduction, the reduction in wustite scale had a distinct difference and advantage, which is the presence of a steel substrate as an iron core between the scale layers. The results observed in the current study revealed that the iron core had promoted the reduction process by allowing iron ions to diffuse through the wustite layer and deposit on it, thus maintaining a very thin iron layer on the surface. Eq. (7') shows that if the iron layer thickness  $x$  remains very thin, a relative large and constant iron flux can be maintained even when both  $D_{\text{O}}^{\text{Fe}}$  and  $C_{\text{O}}^{\text{Fe-FeO}}$  are small.

In the discussion of iron diffusion through the iron layer formed on bulk wustite [30–34], the iron concentration in the metallic iron at the wustite–iron interface was always assumed to be the saturated oxygen concentration in equilibrium with the thermodynamically stable wustite phase at the reaction temperature, having a nearly constant composition of about  $\text{Fe}_{0.95}\text{O}$  [11] (Fig. 15). This condition would be automatically fulfilled if the oxygen flux diffusing away from the interface was not too large, as schematically shown in Fig. 18a.

However, in the situation where the oxygen flux diffusing away from the iron–wustite interface was large (especially when  $x$  is very small) and exceeded the supply rate of oxygen released from the wustite phase through the following interface reaction (Fig. 17),



the oxygen concentration at the interface on the iron side would be lowered to one less than the saturated oxygen concentration in equilibrium with the thermodynamically stable wustite. Corresponding to this oxygen concentration reduction, if

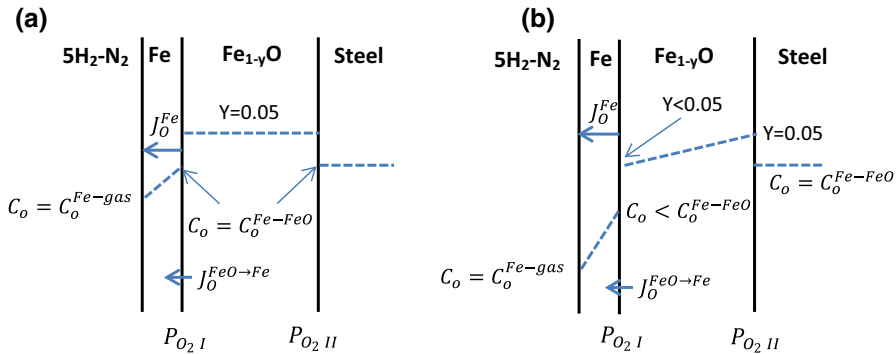


**Fig. 18** Two scenarios of the Fe–Fe<sub>1-y</sub>O interface conditions: **a** when the oxygen flux diffusing away from the Fe–FeO interface  $J_O^{Fe}$  is low and the iron flux crossing the FeO–Fe interface  $J_O^{FeO→Fe}$  via Reaction 8 is sufficiently high to maintain the saturated iron concentration at the interface ( $C_o = C_o^{Fe-FeO}$  in equilibrium with Fe<sub>0.95</sub>O),  $P_{O_2I} = P_{O_2II}$ . In this case, there is no driving force for iron to diffuse through the wustite layer, **b** when the oxygen supply rate crossing the FeO–Fe interface  $J_O^{FeO→Fe}$  via Reaction 8 is relatively low, the interface oxygen concentration of the iron layer will be lowered to  $C_o < C_o^{Fe-FeO}$  to meet the condition of  $J_O^{Fe} = J_O^{FeO→Fe}$ , in this case,  $P_{O_2I} < P_{O_2II}$  which will become a driving force for iron diffusion from the outer Fe–FeO interface to the inner FeO–steel interface.  $P_{O_2I}$  and  $P_{O_2II}$  are the oxygen potentials at the outer Fe–FeO and inner FeO–Fe interfaces, respectively

local equilibrium is still established at the interface, the oxygen concentration of the wustite at the interface would be also lowered to a level corresponding to a metastable wustite phase containing supersaturated iron with a lower oxygen activity or lower oxygen potential. In this way, an oxygen potential gradient is established between the two wustite–iron interfaces, as illustrated in Figs. 18b and 19.

Applying Wagner’s oxidation theory [20, 21, 40] to the current situation, when an oxygen potential difference  $P_{O_2II} - P_{O_2I}$  is established between the two interfaces of the wustite layer, iron will diffuse from one interface to another. When  $P_{O_2II} < P_{O_2I}$ , iron diffuses outward as in steel oxidation, and when  $P_{O_2II} > P_{O_2I}$ , it would be expected that iron would diffuse inwards, as also suggested by Hoar [20] in Fig. 14.

Based on above discussion, we believed that (1) the very thin nature of the iron layer formed on the wustite surface observed in the current study had allowed iron to diffuse rapidly through it, thus lowering the oxygen concentration/potential at the outer iron–wustite interface and provided a driving force for iron diffusion through the wustite layer, and (2) diffusion of iron through the wustite layer had allowed the surface iron layer to maintain its very thin nature, thus maintaining a relatively rapid reduction process, much more rapid than that of bulk wustite reduction.

Clearly, when this mechanism was in operation and the system reached a quasi-steady state as termed by Wagner [21], the wustite layer across its thickness would be all supersaturated with iron with the degree of supersaturation decreasing towards the inner wustite–iron interface. Under such a situation, any outbursts of metallic iron from the inner wustite–iron interface into the wustite layer (as a result of iron deposition at this interface) would be growing at an even more rapid speed

because the further they grew, the higher the degree of iron supersaturation in the wustite phase these outburst fronts would encounter. The growth of these outbursts then relied not only upon iron diffusion from the outer iron–wustite interface, but also from the precipitation of supersaturated iron from the surrounding wustite phase. This explains the reason why an undulating inner wustite–iron interface always developed in the reduction process, as shown in Figs. 8, 9, 10, 11, 12, 13, 17 and 19. In addition, metallic iron nucleation and growth within the metastable wustite layer would be also possible. Such nucleation and growth have been also seen in the scale structures shown in Figs. 8a, b, 9a, b, d, 10b, c and 11d.

From the Arrhenius plots of the kinetics data in Fig. 7, it can be seen that the diffusion mechanisms controlling the reduction process were different at different temperature ranges for both the centre and near-edge samples. At the range of 650–750 °C, the activation energies were 259.8 and 264.5 kJ mole<sup>-1</sup> for the two groups of samples, respectively. These values are close to that for oxygen diffusion in  $\alpha$ -Fe, which is 238.5 kJ mole<sup>-1</sup> [41, 42], suggesting that outward oxygen diffusion through the newly formed iron layer was likely the control mechanism. Under these conditions, it appeared that once a steady state (surface iron layer thickness and interface equilibrium) was established, the rate of oxygen diffusion through the iron layer determined the reduction rate and controlled the reduction process.

At the range of 750–850 °C for the reduction of the centre location samples, the activation energy was significantly lower at 138.5 kJ mole<sup>-1</sup>. This value was close to that for iron diffusion in wustite, which was in the range of 122.9–143.3 kJ mole<sup>-1</sup> [43–45]. The activation energy for the reduction of the near-edge location samples at 750–850 °C was even lower at 73.55 kJ mole<sup>-1</sup>. Iron diffusion in wustite does not result in direct weight loss from the scale samples and would not have a direct contribution on the reduction kinetics. Its contribution probably was made through affecting the rate of interface reaction represented by Eq. 8 and consequently affecting the oxygen concentration of iron at the interface and finally the diffusion rate of oxygen through the iron layer according to Eq. 7.

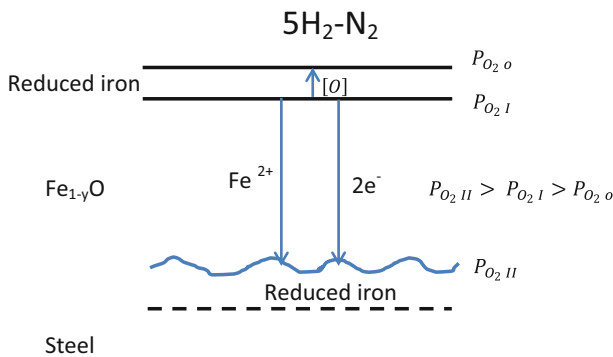


**Fig. 19** Schematic illustration of wustite reduction to iron controlled by oxygen diffusion through the surface iron layer, assisted by iron diffusion across the wustite layer to maintain a thin iron layer on the surface



Namely, a greater iron flux through the wustite layer would lead to lower supersaturation of iron or greater oxygen concentration in wustite at the interface and hence increased interface reaction rate to release oxygen into the adjacent iron phase. This in turn would increase the oxygen concentration in the surface iron layer at the interface, thus increasing oxygen flux through the surface iron layer. At the same time, as more iron had diffused away through the wustite layer, less iron became available to grow the surface iron layer, thus maintaining a thin iron layer on the surface and a steeper oxygen flux to the surface. On the other hand, a decreased iron flux through the wustite layer would lead to greater supersaturation of iron or decreased oxygen concentration in the wustite phase at the iron–wustite interface and hence lower rate of interface reaction to release oxygen into the iron phase. At the same time, more iron became available to grow the surface iron layer, increasing its thickness. In this way, the overall reduction rate is decreased.

The reduction rates at 900 °C for both groups of samples were slower or at least no greater than those at 850 °C. It is likely that at this temperature, the rate of interface reaction was more rapid, leading to a higher oxygen concentration in the iron phase. Consequently, the oxygen potential difference across the wustite layer was decreased, leading to a decreased iron flux through the wustite phase. As a result, the surface iron layer thickness was increased, as shown in Fig. 12d, e, and consequently, oxygen flux diffusing through the iron layer was decreased.

#### (4) Reduction of the remaining wustite islands and porosity formation.

Towards the end of the reduction process, with further outward migration of the undulating inner wustite–iron interface, most of the wustite layer was reduced to iron with only some isolated wustite islands left, as schematically shown in Fig. 20.

Loss of oxygen from the wustite islands resulted in their volume shrinkage and generated cavities adjacent to them. Once cavities were generated, hydrogen transport through the reduced iron layer then could play a part in the reduction process because the product of its reaction with wustite (water vapour) could now be

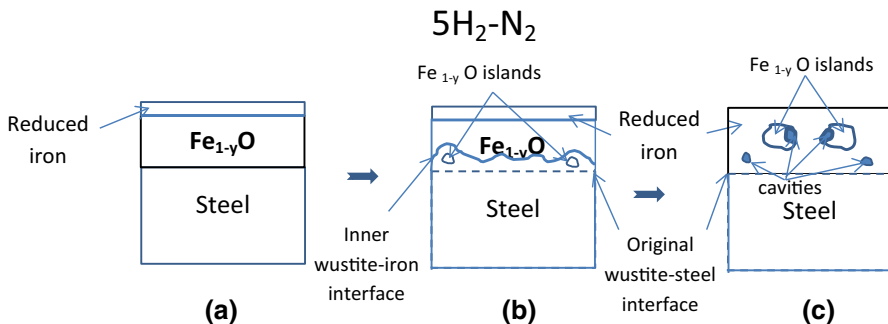


**Fig. 20** Schematic illustration of various stages in the reduction in wustite: **a** initial stage with the formation of a surface iron layer, **b** early stage with the outward migration of the inner wustite–reduced iron interface, leaving some small wustite islands behind and **c** most of the wustite layer was reduced, with some remaining wustite islands (attached with cavities) left behind. Small cavities were formed after the small wustite islands were reduced to iron

stored in the cavities, as illustrated in Fig. 21. It is well known that iron is permeable to hydrogen gas and as discussed earlier, hydrogen diffusion is rapid [25–28]. It was therefore possible for hydrogen to diffuse through the several micron thick iron layer to occupy the cavities generated and participate in the reduction process.

From the microscopic point of view, the diffusion processes and reactions illustrated in Figs. 17 and 19 also apply to the reduction process of wustite islands by hydrogen gas stored in the cavities. However, it must be noted that if the reaction product water vapour is also stored in the cavity, then there is no net weight loss of the sample and the reaction kinetics would not be detectable using the weight loss method, and more importantly, once sufficient water vapour is generated, the reduction reaction according to Eq. 6 will cease when the arriving hydrogen gas and the generated water vapour reach equilibrium. For the reduction process to continue, oxygen must be diffusing away from the cavities or from the surface of the wustite islands, and therefore, the control mechanism of this final stage was most likely the outward diffusion of oxygen through the reduced iron layer. When some of the wustite islands were buried deep in the reduced iron layer, the final process would become tedious because the rate of oxygen diffusion through a thick iron layer would be very slow, as discussed earlier.

#### (5) Effect of scale structure on the reduction rate.

From the kinetics results, it is clear that the reduction rates of the near-edge samples were constantly lower than those of the centre samples. Repeated experiments at a later study [46] have confirmed these observations, as illustrated in Fig. 22 where the reduction kinetics at 850 °C in 5% $H_2$ - $N_2$  under a gas flow of 3 L  $min^{-1}$  is presented.

To assist in the discussion, the evolution of oxygen concentration gradient in the wustite layer of a near-edge sample in a reduction process is illustrated in Fig. 23.

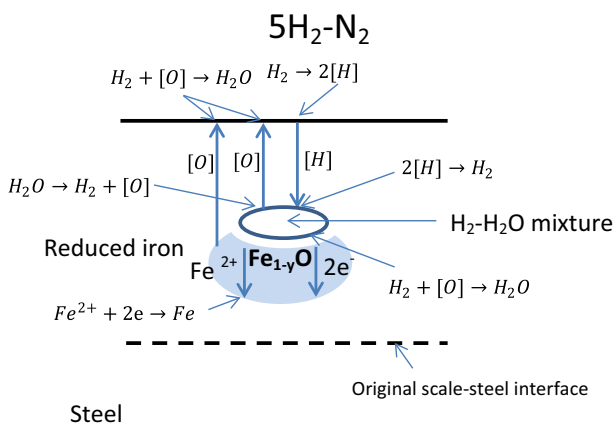


**Fig. 21** Schematic illustration of cavity formation as a result of wustite island reduction. For the reaction and diffusion process at or through the thin iron layer between the cavity and the wustite phase (not shown), refer to Figs. 17 and 19

**Fig. 22** Comparison of the reduction rates of centre and near-edge location scales at 850 °C in 5% $H_2$ - $N_2$  flowing at a rate of 3 L  $min^{-1}$  [46]

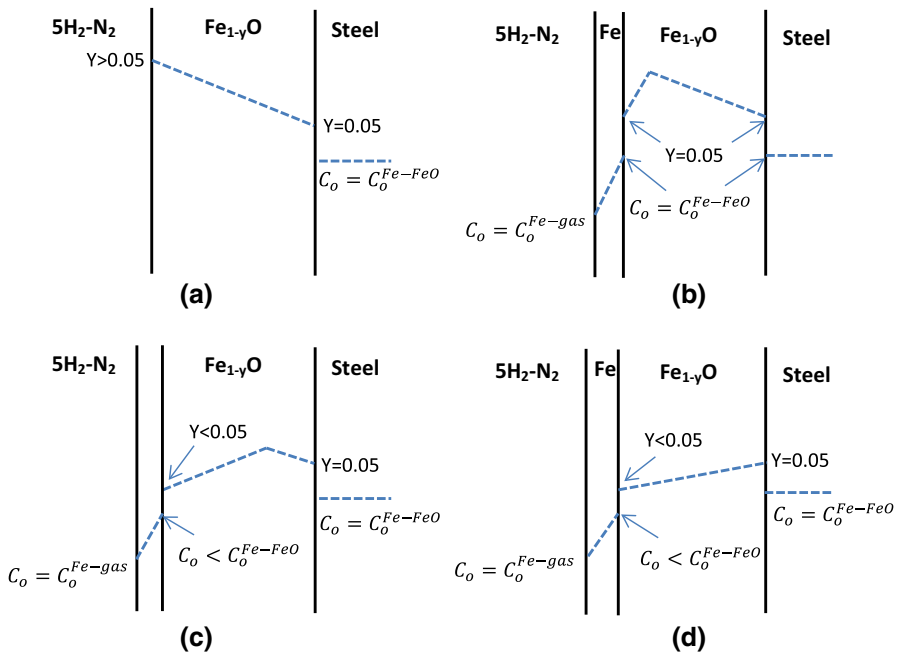
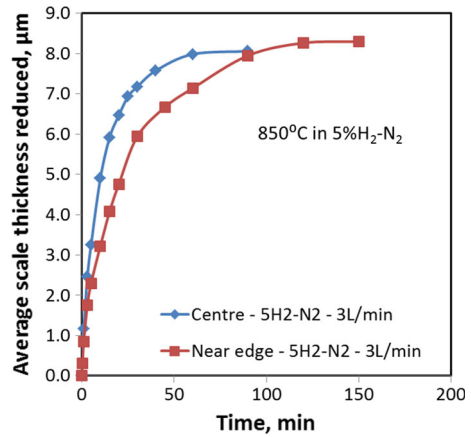
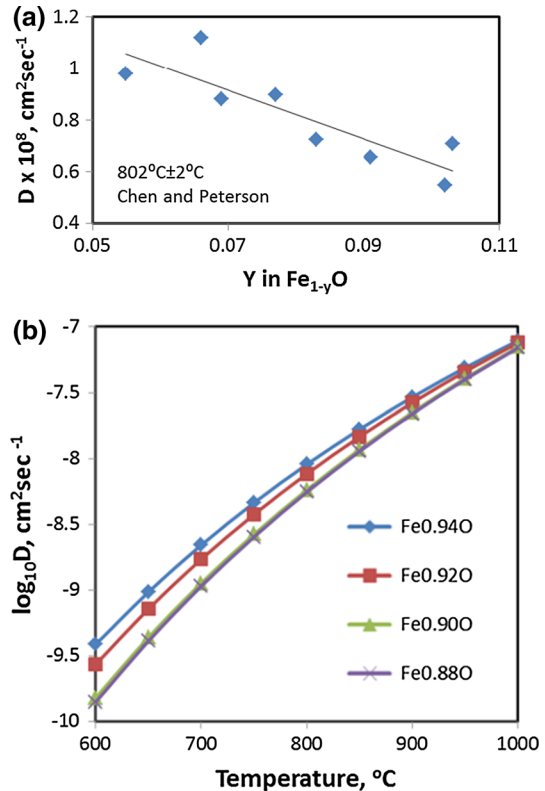


**Fig. 23** Schematic illustration of oxygen concentration gradient evolution in the wustite layer on a near-edge sample: **a** initial stage—two-layered scale structure transformed into wustite. The entire wustite layer was oxygen rich ( $Y > 0.05$ ) with the highest oxygen concentration on the surface: **b** very early stage—reduction with 5 $H_2$ - $N_2$  gas, forming an iron layer on the surface. The oxygen concentrations on both sides of the interface were determined by the FeO–Fe equilibrium, but the majority of the wustite layer was still oxygen rich ( $Y > 0.05$ ), **c** later stage—the rate of interface reaction to release oxygen into the iron phase could not keep up with rapid diffusion of oxygen away from the Fe–FeO interface, and therefore, the oxygen concentrations on both sides of the interface were lowered to the levels below those determined by the FeO–Fe equilibrium. However, the inner part of the wustite layer was still oxygen rich, and **d** much later stage—the oxygen concentrations across the wustite layer were decreased to levels lower than that determined by the FeO–Fe equilibrium, reaching the state that was similar to the initial state of centre sample reduction. A composition of  $Fe_{0.95}O$  ( $Y = 0.05$ ) is approximated as the thermodynamically stable wustite at all temperatures [11]

**Fig. 24** Relationship between the self-diffusion coefficient of iron in wustite  $\text{Fe}_{1-y}\text{O}$  and the degree of deviation from stoichiometry: **a** experimental data at 802 °C [40] and **b** extrapolated to a wider temperature range [44, 45]



As discussed earlier, the initial oxygen concentration gradient in the wustite scale of the near-edge samples is different from that in a centre location sample, as shown in Fig. 23a, with the oxygen concentration at the surface being the highest. With its higher oxygen concentration on the surface (than that in the centre samples), the duration for it to become iron rich (supersaturated with iron) is longer.

After the formation of the surface iron layer, the rate of further reduction is determined by the rate of oxygen diffusion away from the iron–wustite interface, and the excess iron released at the surface layer of the wustite will first to diffuse into the wustite layer to lower the oxygen concentrations in the oxygen-rich regions, as shown in Fig. 23b, c, before depositing at the inner FeO–Fe interface (Fig. 23d). Note that for the convenience of illustration,  $Y = 0.05$  is used in Fig. 23 to represent the wustite concentration that is in equilibrium with the adjacent metal iron phase at any reaction temperature. Once the concentration gradient is changed to that shown in Fig. 23d, further reduction process will follow a similar trend to that of the centre location sample. The additional steps required to reach the state of centre location sample reduction should account for most of the longer reduction duration required.

Different iron diffusivities in the two wustite structures could also have some contributions to the different reduction rates observed. From the experimental results of Chen and Peterson [44, 45], the self-diffusion coefficient of iron in wustite

is a function of wustite composition, decreasing with increased oxygen concentration. The effect is more significant at 800 °C (Fig. 24a) than at 1000–1200 °C and could be more significantly at even lower temperatures, as shown in Fig. 24b [45]. It is seen that at 800 °C the self-diffusion coefficient of iron in wustite was reduced by half when the  $y$  value was increased from 0.055 ( $\text{Fe}_{0.945}\text{O}$ ) to 0.102 ( $\text{Fe}_{0.898}\text{O}$ ).

## Conclusions

This study examines the reduction behaviour of oxide scale on hot-rolled, low-carbon steel in flowing 5% $\text{H}_2$ - $\text{N}_2$  gas at 650–900 °C, leading to the following conclusions:

1. The reduction behaviour of the scale at different locations was similar, but the centre location scale was reduced more rapidly than the near-edge location scale.
2. The reduction rates for both groups of scale at 650 °C were very low, increased with increased temperature, reached their maxima at 850 °C and then decreased slightly again at 900 °C.
3. The shortest durations required to achieve nearly complete reduction at 850 °C were 20 and 45 min for the scales at the centre and near-edge locations, respectively.
4. Under all conditions, a very thin iron layer quickly formed at the very beginning of the reaction (<20 s for the centre location samples and no more than 2 min for the near-edge samples) and the subsequent reduction process proceeded via outward migration of the scale–steel interface.
5. Iron diffusion through the wustite layer to deposit on the steel substrate allowed the very thin nature of the surface iron layer to be maintained. It was believed that the more rapid oxygen diffusion rate through the thin surface iron layer than the oxygen release rate through the iron–wustite interface reaction resulted in a lower oxygen potential at the outer iron–wustite interface, thus providing a driving force for iron ions to diffuse through the wustite layer.
6. Judging from the activation energies obtained, oxygen diffusion through the surface iron layer was the control mechanism for both the centre and near-edge samples at 650–750 °C, whereas iron diffusion through the wustite layer was likely the control mechanism at 750–850 °C.
7. At 900 °C, the iron–wustite interface reaction could be more rapid, leading to higher oxygen concentration in the surface iron layer at the interface, reduced iron flux through the wustite layer and therefore a thicker iron layer on the surface. As a result of this, the reduction rate became even lower than that at 850 °C.
8. Higher oxygen concentrations in the initial wustite phase in the near-edge samples are believed to be responsible for the much lower reduction rates than those of the centre location samples.
9. The final stage of slow reduction of both types of scale was most likely controlled by oxygen diffusion through the reduced iron layer to the surface to

reduce the remaining wustite islands embedded. Porosities were generated as a result of reduction of the isolated wustite islands.

**Acknowledgements** Permission from the management of BlueScope Limited for publication of the information contained in this paper is gratefully acknowledged.

## References

1. N. L. Samways, Hydrogen descaling of hot band: a competitor to acid pickling. *Iron and Steelmaker* **28**, (11), 23–26 (2001).
2. WO 01/91929 A1, *Apparatus and Method for Sequential Removal of Oxides from Steel*, Applicant: Danieli Technology, Inc.; Inventor: Stephen L. Feldbauer and Brian Braho (2001).
3. A. Primavera, S. Cattarino and M. Pavlicevic, Influence of process parameters on scale reduction with H<sub>2</sub>. *Ironmaking and Steelmaking* **34**, 290–294 (2007).
4. M. Picard (Arcelor), M. van den Eynde (CRM), N. Zachetti (CSM), J. Kömi and M. Lehtinen (Ruukki), *Control of Surface Layer for Pickle-Free Hot-Rolled Strip*, European Commission Technical Steel Research—2008 EUR 22852 EN.
5. J. Shi, D. Wang, Y. He, H. Qi and W. Gao, Reduction of oxide scale on hot-rolled strip steels by carbon monoxide. *Materials Letters* **62**, 3500–3502 (2008).
6. I. Saeki, T. Ikeda, K. Ohno, T. Sato and S. Kurosawa, Reduction of oxide scales formed on low carbon steel sheet in synthesized combustion gas. *Tetsu-to-Hagané* **97**, (1), 12–18 (2011).
7. C. Guan, J. Li, N. Tan, Y.-Q. He and S.-G. Zhang, Reduction of oxide scale on hot-rolled steel by hydrogen at low temperature. *International Journal of Hydrogen Energy* **39**, 15116–15124 (2014).
8. C. Guan, J. Li, N. Tan and S.-G. Zhang, Continuous reduction of the oxide scale of hot rolled steel strip in hydrogen. *Ironmaking and Steelmaking* **43**, 739–743 (2016).
9. Y. He, T. Jia, Z. Li, G. Cao and Z. Liu, Isothermal reduction of oxide scale on hot-rolled low-carbon steel in 10 Pct H<sub>2</sub>-Ar. *Metallurgical and Materials Transactions A* **47**, 4845–4852 (2016).
10. R. Y. Chen and W. Y. D. Yuen, oxide-scale structures formed on commercial hot-rolled steel strip and their formation mechanisms. *Oxidation of Metals* **56**, 89–118 (2001).
11. R. Y. Chen and W. Y. D. Yuen, Review of the high-temperature oxidation of iron and carbon steels in air or oxygen. *Oxidation of Metals* **59**, 433–468 (2003).
12. Z. Liu, G. Cao, Y. He, M. Yang and Z. Liu, Reduction of oxide scale with hydrogen. *International Journal of Iron and Steel Research* **21**, (1), 24–29 (2014).
13. Y.-Q. He, T. Jia, X.-J. Liu, G.-M. Cao, Z.-Y. Liu and J. Li, Hot-dip galvanizing of carbon steel after cold rolling with oxide scale and hydrogen descaling. *International Journal of Iron and Steel Research* **21**, (2), 222–226 (2014).
14. Pohang Iron & Steel Co. Ltd (KR) (inventors: Kyungsangbook-do Jin Won Choi), *Method for manufacturing hot rolled galvanized steel sheet at high speed, with pickling skipped*, US 6258186 B1 (2001).
15. R. Y. Chen and W. Y. D. Yuen, Oxide scales on hot-rolled steel strips. in *Developments in High-Temperature Corrosion and Protection of Materials*, eds. W. Gao and Z. Li (Woodhead Publishing Limited, Cambridge, 2008), pp. 192–252.
16. R. Y. Chen and W. Y. D. Yuen, Oxidation of low-carbon steel in 17H<sub>2</sub>O–N<sub>2</sub> at 900 °C. *Metallurgical and Materials Transactions A* **40A**, 3091–3107 (2009).
17. O. H. Gellner and F. D. Richardson, Reduction of ferrous oxide. *Nature* **168**, 23–24 (1951).
18. E. T. Turkdogan and J. V. Vinters, “Gaseous reduction of iron oxides: part III. Reduction-oxidation of porous and dense iron oxides and iron. *Metallurgical Transactions* **3**, 1561–1574 (1972).
19. F. D. Richardson and E. Dancy, *The Physical Chemistry of Process Metallurgy: Discussion of the Faraday Society*, 1948, Vol. 4, pp. 229–230, Butterworths, London (1961).
20. T. P. Hoar, *The Physical Chemistry of Process Metallurgy: Discussion of the Faraday Society*, 1948, No. 4, p. 230, Butterworths, London (1961).
21. C. Wagner, Mechanism of the reduction of oxides and sulphides to metals. *Transactions of the American Institute of Mining and Metallurgical Engineers* **194**, 214–216 (1952).

22. J. O. Edström, The mechanism of reduction of iron oxides. *Journal of the Iron and Steel Institute* **188**, 289–304 (1953).
23. H. A. Wriedt, Fe–O (Iron–Oxygen). in *Binary Alloy Phase Diagrams*, vol. 2, 2nd ed, eds. T. B. Massalski, H. Okamoto, P. R. Subramanian and L. Kacprzak (ASM International, Metals Park, 1990), pp. 1739–1744.
24. R. Y. Chen and W. Y. D. Yuen, Improvement of pickling characteristics of hot-rolled strip through heat treatment of the oxide scale. *Iron and Steelmaker* **30**, (3), 17–22 (2003).
25. H. J. Grabke and E. Riecke, Absorption and diffusion of hydrogen in steels. *Materiali in Tehnologije* **34**, 331–342 (2000).
26. N. Shohoji, Comparative study of solubilities of hydrogen, nitrogen and carbon in  $\alpha$ -iron. *Journal of Materials Science* **21**, 2147–2152 (1986).
27. G. E. Murch, *Diffusion in Solids—Unsolved Problems*, (Trans Tech Publications, Switzerland, 1992), p. 103.
28. H. Hagi, Diffusion coefficient of hydrogen in iron without trapping by dislocation and impurities. *Materials Transactions, JIM* **35**, (2), 112–117 (1994).
29. R. Kirchheim, Bulk diffusion-controlled thermal desorption spectroscopy with examples for hydrogen in iron. *Metallurgical and Materials Transactions* **47A**, 672–696 (2016).
30. P. C. Hayes, Analysis of product morphologies and reaction mechanisms on gaseous reduction of iron oxides. *Steel Research International* **82**, 480–493 (2011).
31. S. el Moujahid and A. Rist, The nucleation of iron on dense wustite: a morphological study. *Metallurgical Transactions B* **19B**, 787–802 (1988).
32. M. Farren, S. P. Mathew and P. C. Hayes, Reduction of solid wustite in  $H_2/H_2O/CO/CO_2$  gas mixtures. *Metallurgical Transactions B* **21B**, 135–139 (1990).
33. D. H. St. John, S. P. Mathew and P. C. Hayes, The breakdown of dense iron layers on wustite in  $CO/CO_2$  and  $H_2/H_2O$  systems. *Metallurgical Transactions B* **15B**, 701–708 (1984).
34. D. H. St. John and P. C. Hayes, Microstructural features produced by the reduction of wustite in  $H_2/H_2O$  gas mixtures. *Metallurgical Transactions B* **13B**, 117–124 (1982).
35. J. H. Swisher and E. T. Turkdogan, Solubility, permeability, and diffusivity of oxygen in solid iron. *Transactions of the Metallurgical Society of AIME* **239**, 426–431 (1967).
36. J. Takada, S. Yamamoto, S. Kikuchi and M. Adachi, Determination of diffusion coefficient of oxygen in  $\gamma$ -iron from measurement of internal oxidation in Fe–Al alloys. *Metallurgical Transactions A* **17A**, 221–229 (1986).
37. J. Takada, S. Yamamoto, S. Kikuchi and M. Adachi, Internal oxidation of Fe–Al alloys in the  $\alpha$ -phase region. *Oxidation of Metals* **25**, 93–105 (1986).
38. J. Takada and M. Adachi, Determination of diffusion coefficient of oxygen in  $\alpha$ -iron from internal oxidation measurements in Fe–Si alloys. *Journal of Materials Science* **21**, 2133–2137 (1986).
39. J. Takada, K. Kashiwagi and M. Adachi, Internal oxidation of Fe–Si alloys in  $\gamma$ -phase region. *Journal of Materials Science* **19**, 3451–3458 (1984).
40. C. Wagner, *Diffusion and high temperature oxidation of metals*, (American Society for Metals, Cleveland, Ohio, Atom Movements, 1951), pp. 153–173.
41. L. Bogdandy and H.-J. Engell, *The Reduction of Iron Ores*, (Springer, New York, 1971), p. 135.
42. H. K. Kohl and H.-J. Engell, Reduction of wustite in hydrogen. *Archiv für das Eisenhüttenwesen* **34**, 411–418 (1963).
43. L. Himmel, R. F. Mehl and C. E. Birchenall, Self-diffusion of iron in iron oxides and the Wagner theory of oxidation. *Journal of Metals (Transactions AIME)* **5**, 827 (1953).
44. W. K. Chen and N. L. Peterson, Effect of the deviation from stoichiometry on cation self-diffusion and isotope effect in wustite,  $Fe_{1-x}O$ . *Journal of Physics and Chemistry of Solids* **36**, 1097–1103 (1975).
45. R. Y. Chen and W. Y. D. Yuen, Longer term oxidation kinetics of low carbon, low silicon steel in  $17H_2O-N_2$  at 900 °C. *Oxidation of Metals* **85**, 489–507 (2016).
46. R. Y. Chen, Reduction kinetics of iron oxide scale in  $5-15\%H_2-N_2$  at 850 °C, to be submitted to *Oxidation of Metals* (2017).